American College of Neuropsychopharmacology

www.nature.com/npp

ARTICLE OPEN

Check for updates

Visual attention is linked to temporally structured noradrenaline release in the medial prefrontal cortex

Leonie P. Posselt[1], Júlia Coll-Marquès[1], Samuel Ovrom[1], Søren H. Jørgensen[1], Sebastian H. Eliassen[1], Katharina Kliem[1], Jennifer Müller[1], Jeffrey W. Dalley[2,3,4], Trevor W. Robbins[2,3], Freja Herborg[1], Andreas T. Sørensen[1] and Ulrik Gether[1]✉

Visual attention enables filtering of irrelevant stimuli and focus on information that is most pertinent to survival. While the locus coeruleus-noradrenaline (LC-NA) system is recognized as crucial in this process, the role of temporally structured NA signaling in visual attentional performance remains unsettled. Here, by using the genetically encoded NA sensor $GRAB_{NE2h}$ together with fiber photometry in mice, we identify sub-second NA release signatures in the medial prefrontal cortex (mPFC) that correlate with visual attention accuracy in the rodent Continuous Performance Test (rCPT). The dual-peak release signatures were time-locked to correct, rewarded responses, preceded by a ramp-up after stimulus presentation and followed by a decline at reward collection. No such signatures accompanied misses, correct rejections and mistakes. Similar, albeit less pronounced, patterns were observed in the lateral hypothalamus (LH). Activation of the Gq-coupled DREADD (Designer Receptors Exclusively Activated by Designer Drugs) hM3DGq expressed in LC neurons dose-dependently increased tonic NA levels in both mPFC and LH, while simultaneously distorting phasic NA signatures and impairing rCPT performance without affecting locomotor activity. Summarized our data suggest that NA enhances alertness to reward-associated stimuli through precise, dynamic release patterns underscoring its role in modulating attentional performance beyond tonic signaling.

Neuropsychopharmacology; https://doi.org/10.1038/s41386-026-02404-3

INTRODUCTION

To ensure survival both humans and animals must continuously adapt to changes in the environment and take appropriate actions. This process requires allocation of mental resources to focus on certain aspects of the surroundings while ignoring others. Substantial evidence highlights a central role of the locus coeruleus (LC) [1–3], a nucleus in the pons that serves as the primary source of noradrenaline (NA) [2, 3]. This nucleus provides extensive innervations throughout the brain, delivering NA to regions involved in attention, arousal, decision-making, motor control, and stress responses, [3–12]. Overall, the NA network is believed to maintain the balance between filtering out irrelevant information and prioritizing relevant cues, thereby influencing cognitive functions [6, 13–15]. Prior work shows that both insufficient and excessive NA disrupt top-down control and attention [4, 5, 16–20], which has led to the suggestion of an inverted U-shaped relationship where both too low and too high levels of NA are associated with impaired cognitive performance [1, 5, 12, 17, 21, 22]. This balance is critical in neuropsychiatric disorders such as attention-deficit hyperactivity disorder (ADHD), where dysregulated NA transmission is assumed to contribute to inattention and impulsivity [23, 24]. Importantly, ADHD first-line treatment involves psychostimulants, such as amphetamines or methylphenidate, that increase catecholamine levels via their interactions with the NA and dopamine transporters [25–27].

The neuronal projections from LC to the medial prefrontal cortex (mPFC) are thought to play a specific role in modulating attention and impulse control [28–30], with the prelimbic medial PFC (PrL mPFC) implicated in sustained attention and behavioral flexibility [31–33]. While the effect of NA depletion via pharmacological interventions or lesions has been extensively studied [30, 34–36], it remains unclear how NA release is temporally structured in the PrL mPFC during attentional performance and to what extent the performance depends on precisely timed, task-locked (phasic) NA release as opposed to elevated overall (tonic) NA levels [37]. Moreover, the precise nature of neural coordination between the LC and the mPFC remains poorly understood. Interestingly, optogenetic manipulations recently showed that LC stimulation enhances goal-directed attention, whereas inhibition increases distraction and impulsivity [38]. In addition, recent electrophysiological investigations, as well as two-photon fluorescent imaging experiments, have hinted further at the importance of coordinated neural activity within the LC-prelimbic cortex circuit for optimal attentional performance [11, 37], but how such LC activity patterns translate into NA release dynamics during task performance remains largely unknown.

A limitation in understanding the precise role of NA in attentional processes has been the lack of tools capable of capturing real-time NA dynamics and at the same time manipulating them in a temporal manner in freely moving animals. To

[1]Department of Neuroscience, Faculty of Health and Medical Sciences, University of Copenhagen, DK-2200 Copenhagen, Denmark. [2]Behavioural and Clinical Neuroscience Institute, University of Cambridge, Cambridge CB2 3EB, UK. [3]Department of Psychology, University of Cambridge, Cambridge CB2 3EB, UK. [4]Department of Psychiatry, University of Cambridge, Cambridge CB2 0SZ, UK. ✉email: gether@sund.ku.dk

Received: 18 November 2025 Revised: 19 March 2026 Accepted: 23 March 2026
Published online: 08 April 2026

address this, we employ the recently developed, genetically encoded NA biosensor $GRAB_{NE}$ (G-protein-coupled receptor activation-based NA) sensor [39, 40] in combination with fiber photometry and Designer Receptors Exclusively Activated by Designer Drugs (DREADDs) [41, 42]. This enabled direct assessment in mice of NA release in mPFC, with and without chemogenetic LC activation, during the rodent Continuous Performance Test (rCPT), a learned visual attentional task proposed as a translational paradigm for comparative studies between humans and rodents [24, 37, 43–45]. As a subcortical control, we also included measurements in the lateral hypothalamus (LH). Summarized, our findings both reinforce the role of tonic NA levels in attentional regulation and establish a direct link between the precise temporal structure of NA release and visual attentional performance.

METHODS

Mice

Male adult TH-$Cre^{+/-}$ C57BL/6 J mice were generated by Dr. Ted Dawson at Johns Hopkins University [46], and were maintained heterozygous by breeding in house with female C57Bl6N mice, supplied from Charles River. Previous work showed that TH-Cre mice exhibit preserved catecholaminergic homeostasis and behavior [47]. All procedures were approved and carried out in accordance with the guidelines of the Danish Animal Experimentation Inspectorate (permission number: 2017-15-0201-01160). See Supplemental Methods for details.

Stereotactic surgeries

Mice (TH-Cre and wildtype (WT) control) were anesthetized using isoflurane and stereotactically injected with adeno-associated virus (AAV) encoding the Gq-coupled DREADD hM3DGq (AAV-hSyn-hM3D(Gq)-mCherry); Addgene viral prep (#50474-AAV8) and/or $GRAB_{NE2h}$ (AAV9-hSyn-$GRAB_{NE2h}$) received as a gift from Dr. Yulong Li, Peking University. For expression of hM3DGq, virus was injected bilaterally in LC above, below and at the target coordinates (AP: -5.4 mm; ML: +/-0.9 mm; DV: -3.75 mm). For expression of $GRAB_{NE2h}$, virus was unilaterally (balanced groups of mice for left and right hemisphere) into PrL mPFC and LH above, below and at the target coordinates (mPFC: AP: 2.10 mm; ML: +/-0.27 mm; DV: -2.30 mm; LH: AP: -1.34 mm, ML: +/-1.10 mm, DV: -4.90 mm). Optic fiber cannulas (MBF Europe B.V., Netherlands) with 1.25 mm ferrule diameter, 200 um fiber core diameter, and 5 mm (for LH) or 2.5 mm (for mPFC) length, were implanted at the target region. See Supplemental Methods for details.

Behavioral tests

All behavioral tests were performed by experimenters blinded to genotypes and in case of drug testing blinded to injected doses.

Open field test. A minimum of three weeks after surgery, mice were individually placed in the middle of a custom-made 50 × 50 × 40 cm white arena and allowed to explore for 45 min before i.p. injection followed by 60 min further exploration. Mice were tested in a cross-over design with 2 mg/kg CNO and vehicle over two days. Tracking and subsequent analysis were performed using EthoVision XT (Noldus).

Rodent continuous performance test (rCPT). The rCPT training was performed with food-restricted mice in touchscreen operant chambers (Campden Instruments, UK). In brief, mice learned to respond to a rewarded target (S +) image and to withhold from responding to non-target stimuli (S-). Recordings were done with ABET II (Campden Instruments) and WhiskerServer software (Cambridge University Technical Services, UK). Mice were trained as indicated through stages 1-4 with gradually increasing complexity using stage-specific criteria adjusted after [43] (Supplementary Table S1). During the training stages, mice were tested daily (5 out of 7 weekdays) for 30 min. A mouse was considered having met criteria in Stage 3 and Stage 4 when reaching a d' parameter ≥ 1 for two consecutive days. Once a mouse reached the criterium, it was trained once a week to maintain optimal performance. See Supplemental Methods for details.

Fiber photometry

Fiber photometric recordings were performed with a Neurophotometrics FP3002 system during the open-field test and selected parts of rCPT using the open-source software Bonsai [48]. Cannula implants of mice were attached to multi branching fiber optic patch cords (Doric Lenses, 200 µm, NA 0.37) with white or bronze mating sleeves (Thorlabs ADAL 4-5). Each channel was recorded at 20 Hz ($GRAB_{NE2h}$, 470 nm channel; isosbestic signal, 415 nm channel). Raw fluorescence measurements were preprocessed by first subtracting the isosbestic signal from the $GRAB_{NE2h}$ signal followed by calculating zF of the resulting signal with the equation $zF = (F-\mu_F)/\sigma_F$, (μ_F = mean value of the fluorescence and σ_F = standard deviation of the fluorescence signal over the baseline period) [49]. The rCPT behavioral data were synchronized to photometry data via TTL time stamps from the operant chambers. See Supplemental Methods for details.

Immunohistochemistry

Mouse brains were transcardially perfused, fixed and sectioned on a cryostat. Resulting coronal sections (40 µm) were immunolabeled with anti-TH antibody (MAB388, Milliprobe; 1:1000), anti-mCherry antibody (ThermoFisher 16D7; 1:2000) and/or anti-GFP antibody (ab13970, Abcam; 1:500) followed by labeling with Alexa Fluor 488 goat anti-mouse secondary antibody (1:400; Abcam), Alexa Fluor 568 goat anti-rat secondary antibody (1:400; Abcam) or Alexa Fluor 647 goat anti-chicken secondary antibody (1:400; Abcam). Brain sections were imaged on a Zeiss Axio Scan Z1 slide scanner.

Statistical analysis

Choice of statistical analysis is presented in the legends associated with each figure. Calculations were carried out using GraphPad Prism 10. Multiple comparisons were corrected for using Tukey's (rCPT) or Sidak's (OFT) tests for post-hoc ANOVA testing. For all analyses, the significance level was set at 0.05, and all behavioral data are presented as the mean ± SD. Photometric data are presented as mean with 95% confidence interval (CI).

RESULTS

Experimental strategy to assess noradrenergic signaling dynamics in mPFC and LH

To investigate NA release dynamics, we unilaterally expressed $GRAB_{NE2h}$ in prelimbic (PrL) mPFC and in LH of TH (tyrosine hydroxylase)-Cre mice and wildtype (WT) mice (Fig. 1A). The LH is, like mPFC, innervated by LC-NA projections and releases NA during stress-related events [50, 51]. Importantly, the LH has been used as a model region to monitor and validate NA release with NA biosensors including $GRAB_{NE2h}$ [40]. We also injected the mice bilaterally in the LC with Cre-dependent Gq-coupled DREADD (hM3DGq) [41, 42] to enable LC-targeted chemogenetic activation in TH-Cre mice (Fig. 1A). Histological verification confirmed strong mCherry expression within the TH-rich LC region; however, some mCherry signal was also observed in peri-LC areas and not all TH + LC neurons showed detectable mCherry (Supplementary Fig. S1A-B). A WT (Cre-negative) control processed in parallel showed TH labeling of the LC but no detectable mCherry signal (Supplementary Fig. S1C). Expression of both hM3DGq (Fig. 1A, left; TH in green, mCherry in red) and the biosensor $GRAB_{NE2h}$ in mPFC (Fig. 1A, top right) and LH (Fig. 1A, bottom right) were verified after all experiments. At least three weeks after surgery, $GRAB_{NE2h}$ fluorescence was recorded through implanted fiber optic cannulae in an open field arena, with and without prior intraperitoneal (i.p.) administration of the DREADD agonist CNO (clozapine N-oxide) [52] (Fig. 1B). Next, all mice were trained in the rCPT involving four different stages of increasing difficulty [43] (Fig. 1B). NA dynamics were photometrically recorded in the first and the last session of each stage. In stage 3, the mice were tested with three different doses of CNO and a vehicle, injected in two replications of a Latin Square Design (Fig. 1B).

Open-field behavior validates chemogenetic LC activation and confirms intact locomotor function

Photometric recordings of both TH-Cre and WT mice during habituation in the open-field arena (Fig. 2A) revealed a stable fluorescent signal from the sensor expressed in mPFC and LH

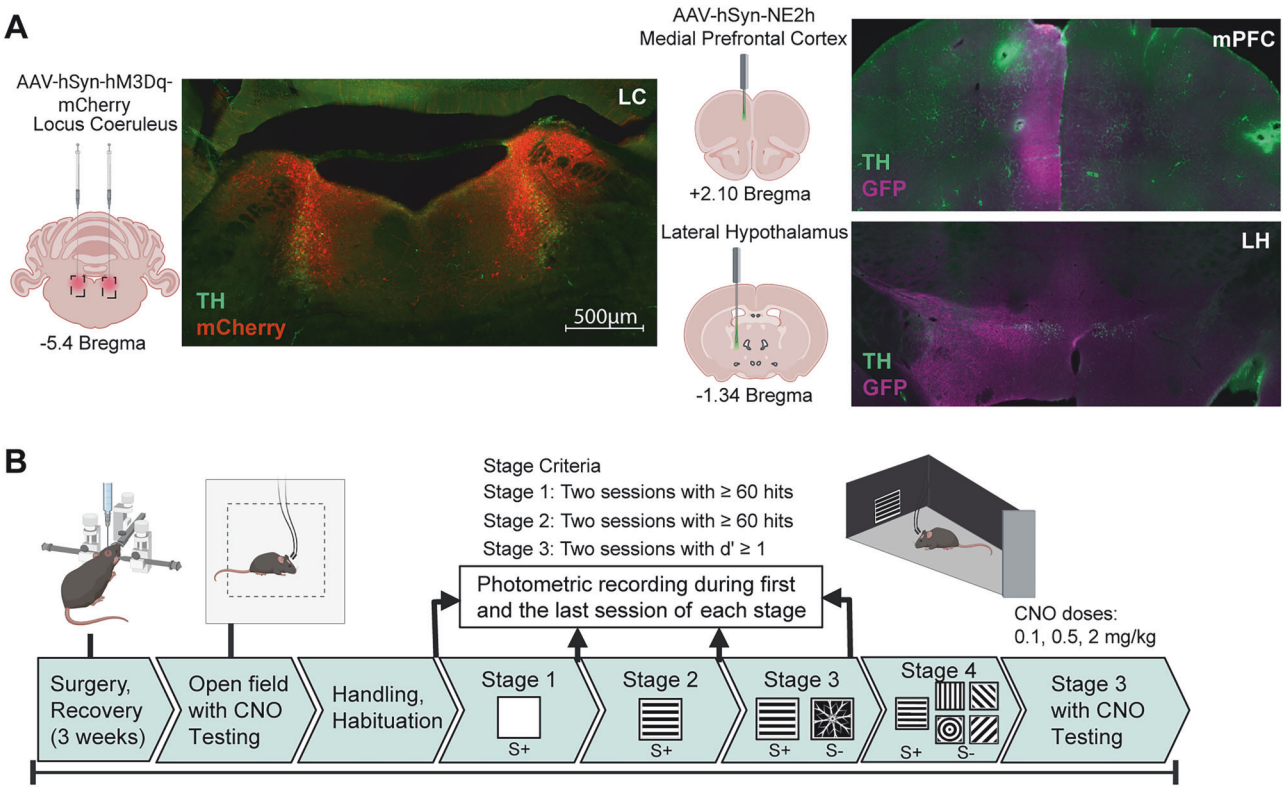

Fig. 1 Experimental strategy. A Left, Schematic of viral injections designed to express the excitatory Gq-DREADD bilaterally in LC, accompanied by an axioscan image at 10x magnification of a LC slice immunostained against TH (green) and mCherry (red). Right Schematic viral injections designed to express $GRAB_{NE2h}$ unilaterally in mPFC or LH, accompanied by an axioscan image of a mPFC and a LH brain slice immunostained for TH (green) and GFP (purple). **B** Timeline of surgeries, open field testing and rCPT training stages and testing. Target and non-target stimuli are indicated for each training stage. In stage 1, the mice learn to associate a screen touch, when a white image is presented, with a reward presented together with sound- and light-cue. In stage 2, the mice learn to associate a specific target stimulus (black horizontal lines on a white background) with reward. In stage 3, mice learn to discriminate between the target stimulus and an unrewarded non-target stimulus presented in the same location, and in stage 4 they learn to discriminate between the target stimulus and 3 different unrewarded non-target stimuli [43]. Arrows indicate when mice were photometrically recorded during training sessions.

(Fig. 2B). Upon administration of CNO (2 mg/kg, i.p.), the signal exhibited a sustained increase persisting throughout the recording period (representative traces in Fig. 2B). In both vehicle and CNO injected mice, we observed at $t = 0$ a peak in fluorescent signal conceivably representing a stress response to the injection (Fig. 2B). The increase upon CNO administration in both mPFC and LH NA signals was consistent across TH-Cre animals while the signal returned to baseline following CNO injection across WT mice (Fig. 2C) and upon vehicle injection in both TH-Cre and WT mice (Fig. 2C). However, it is difficult to compare photometry signal magnitudes across regions and animals, because of potential differences in sensor expression, small differences in fiber placement, and local tissue properties.

Behavioral analysis revealed no differences in total distance traveled, time moved (Fig. 2D, top) or the average velocity between TH-Cre and WT mice (Fig. 2D, bottom left), showing that CNO administration did not impair basic locomotor function. However, the CNO-treated TH-Cre mice spent less time in the center of the arena despite that overall gross movement patterns were preserved (Fig. 2D, bottom right and 2E). This could be indicative of elevated anxiety in the mice resulting from the increased NA levels [53, 54] yet not to a degree that affected the general activity of the mice.

Noradrenergic signaling dynamics in mPFC and LH during rCPT

To study the NA signal during rCPT (Fig. 3A), recordings of both brain regions were synchronized to the start of CPT testing (Fig. 3B) and time-locked to behavioral events during the task (Fig. 3C, D). In the first session of Stage 1, when the mice needed to associate a screen touch (hit) with reward, the mice expectedly only made few hits ($n = 33$). However, an initial signature time-locked to hits was formed in mPFC, characterized by a modest rise beginning prior to a hit and reaching maximum immediately after the hit (Fig. 3C). In the last session of Stage 1, when the mice had learned the task and had many more hits, this increase in mPFC became more defined with an apparent dual peak, the first of which appeared to align with the hit (Fig. 3C).

In Stage 2, where the mice need to recognize a patterned target image (Fig. 3A) a signature in the mPFC developed already during the first training session, with an apparent dual peak (as in Stage 1) followed by a rapid decline in the signal (not seen in Stage 1). The signal decreased below baseline before returning slowly back to baseline within ~5 s (Fig. 3C). In contrast, during the first session of Stage 3, when mice were introduced to a non-target stimulus and had to learn to withhold responding (Fig. 3A), the NA signal appeared less structured (Fig. 3C). By the last session of Stage 3, however, the signature in mPFC became essentially identical to the one seen in last session of Stage 2 (Fig. 3C). The more diffuse NA signature in the first session of Stage 3 might reflect initial uncertainty caused by the introduction of the non-target stimulus image, which also requires an updating of the learned action-outcome association. In comparison, the cognitive demands associated with the transition from Stage 1 to Stage 2 are likely lower, as the change only involves switching from recognizing a white screen to a patterned target image (Fig. 3A). The recordings

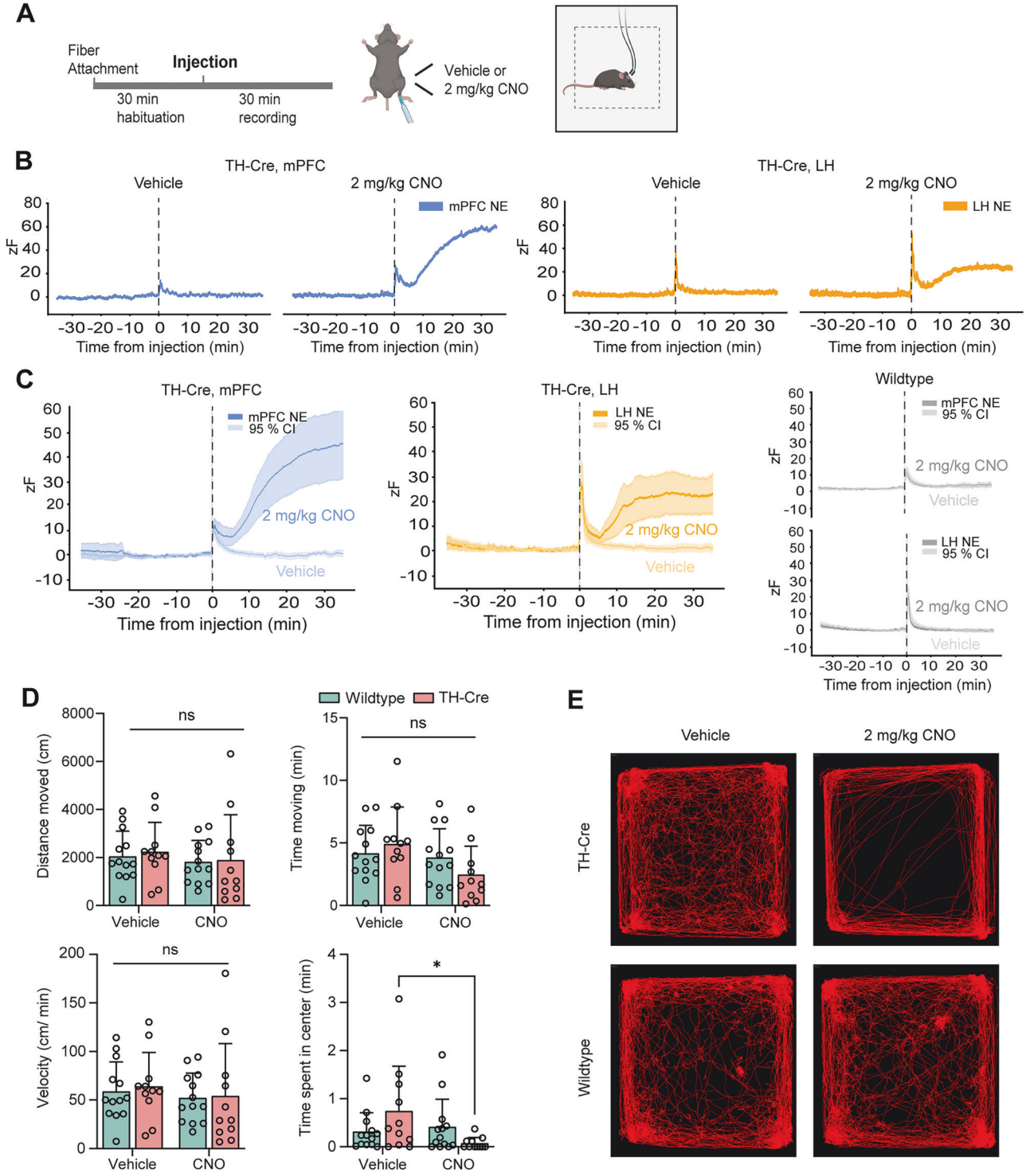

from the LH also showed event-locked increases in NA, but the temporal structure was less defined and lacked the structured dual-peak (Fig. 3C). This might reflect functional differences or differences in LC-derived innervation density between the regions but, as mentioned above, it is difficult to compare absolute photometry amplitudes across regions due to e.g. differences in sensor expression and small differences in fiber placement.

Only a subset of mice ($n = 6$) was further trained in Stage 4, as the number of sessions required to reach the criterion of stage 4 markedly exceeded what we have experienced in previous experiments not involving fiber implants. However, the NA release signatures were very similar to those seen in the last session of stage 3 (Supplementary Fig. S2 and Fig. 4C). These observations are consistent with the introduction of only marginal uncertainty with the transition from Stage 3 to 4. We therefore decided to focus on the fluorescent recordings in stage 3 where all mice had reached the criterion.

We next aligned fluorescence signals during the last session of Stage 3 to reward collection (Fig. 3D). This confirmed a NA signature with a dual peak, with the first peak reaching maximal

Fig. 2 Chemogenetic activation of LC results in increased NA release in mPFC and LH in the open field without affecting gross motor functions. A Open field testing timeline. TH-Cre ($n = 11$) and wildtype ($n = 13$) mice were connected to photometry fibers and placed in the arena for a 30-min baseline recording. After i.p. injection of 2 mg/kg CNO or vehicle, mice were recorded for another 30 min. **B** Representative NA traces (zF) from mPFC (left, blue) and LH (right, orange) in TH-Cre mice, aligned to arena placement (time -30), showing 30 min baseline, injection at time 0, and 30 min post-injection recordings for vehicle and 2 mg/kg CNO conditions. **C** Averaged NA signals (zF) in mPFC (top, blue) and LH (bottom, orange) following vehicle and 2 mg/kg CNO (time 0). Signals are aligned to arena placement (time -30). Shaded areas indicate 95% confidence intervals. **D** Open field test performance following vehicle or 2 mg/kg CNO i.p. (time 0) in TH-Cre (coral) and wildtype (teal) mice. Measures include total distance, time moving, average velocity, and center time, shown as mean ± SD. Sidak-adjusted p-values are reported for within-genotype (vehicle vs. CNO) and between-genotype comparisons, based on two separate repeated-measures two-way ANOVAs ($p < 0.05$ (*), $p < 0.01$, $p < 0.001$, $p < 0.0001$). CNO significantly reduced center time (treatment × genotype: $F(1, 22) = 5.781$, $p = 0.0251$). No significant effects were found for total distance ($F(1, 22) = 0.0217$, $p = 0.8842$), time moving ($F(1, 22) = 2.070$, $p = 0.1643$), or velocity ($F(1, 22) = 0.01795$, $p = 0.8946$). Main effects of treatment and genotype were nonsignificant for all other measures. **E** Overlaid open field locomotor trajectories (red) for TH-Cre (top row) and wildtype (bottom row) mice under vehicle (left) and 2 mg/kg CNO (right). TH-Cre mice showed reduced center exploration after CNO, with no change in wildtype mice.

levels just before the reward collection and the second peak reaching maximum essentially at reward collection. This was followed by a rapid decline in signal as also seen when the signal was aligned to hits (Fig. 3C and D). The changes in fluorescent signals in the LH were similar to those in the mPFC although the signal again was overall more diffuse (Fig. 3D). We also aligned the signal to image presentation prior to a hit, which revealed that the ramp-up of the fluorescent signal seen before the hit in both mPFC and LH (Fig. 3C) occurred immediately after the mice were exposed to the image (Fig. 3D), suggesting that NA release is linked to stimulus evaluation and action preparation.

Finally, signals were aligned to misses (omission of a correct target image), correct rejections (withholding response from non-target image) and false alarms (responding incorrectly to a non-target stimulus). Across these outcomes, we did not observe the prominent, dual-peak hit-associated signature. Any differences, particularly for false alarms, were small and associated with wide 95% confidence intervals, consistent with fewer trials in these categories (Fig. 3D).

Chemogenetic activation promotes NA release and impairs CPT performance

Chemogenetic activation by CNO administration in stage 3 trained mice (Fig. 4A) caused in TH-Cre mice ($n = 6$) but not in WT control mice ($n = 9$) a dose-dependent and significant decrease in active participation, quantified as the total hits and false alarms (Fig. 4B, left). The decline in participation was further substantiated by assessing participation dynamically over time as a rolling performance of participation (Fig. 4C). In contrast, participation under vehicle remained stable (Fig. 4C). In the TH-Cre mice, the classical d′ parameter (calculated as inverse cumulative distribution function [Z-score] of the hit rate and the false alarm rate discrimination [43]) was also significantly and dose-dependently decreased, while WT controls again showed no change (Fig. 4B, right). In parallel, we recorded the NA fluorescence signal showing a strong increase in fluorescence signals in both mPFC and LH of TH-Cre mice, but not in WT mice (Fig. 4D). The increases observed after injection of the lower doses (0.1 and 0.5 mg/kg) were more modest yet still sustained throughout the session (Fig. 4D).

To further substantiate our findings, we investigated a cohort of TH-Cre and WT control mice that were trained in the rCPT to fulfil Stage 4 criteria [43] before they underwent surgery to express Gq-DREADD bilaterally in the LC (Supplementary Fig. S3A and B). This cohort was accordingly not photometrically recorded, and thus any effects of sensor expression and fiber optical implants on performance could be excluded. Similar to our findings for Stage 3, we observed in Stage 4 (Supplementary Fig. S3A and C) a dose-dependent and significant decrease both in task engagement and in the d′ parameter in TH-Cre mice expressing Gq-DREADD but not in WT mice (Supplementary Fig. S3D). In the Variable Stimulus Duration Probe Test (variable SD Test), designed to further challenge attention and impulse control [43], we observed once again reduction in task participation in response to CNO (Supplementary Fig. S3E).

In another experiment, we tested a cohort of TH-Cre and WT mice injected with inhibitory Gi-DREADD [41, 42] bilaterally in the LC (Supplementary Fig. S4A–D). However, despite the Gi-DREADD being expressed in LC (Supplementary Fig. S4C), chemogenetic inhibition with CNO affected neither attentional performance nor the d′ parameter in the rCPT (Supplementary Fig. S4E).

Elevated NA levels disrupt and blunt temporal structure of hit-associated NA signature

Finally, we investigated how elevated NA levels following chemogenetic activation of LC neurons influenced the temporal structure of NA signaling during the rCPT (Fig. 5). These photometry analyses were performed in the chemogenetic cohort (TH-Cre, $n = 6$). When analyzing the data after vehicle injection, the hit-associated NA signature in mPFC described above (Fig. 3C, last session of stage 3) was overall preserved also in this data set (Fig. 5B). However, the dip succeeding the dual peak was reduced (Fig. 5B). Because the only difference between the two data sets was the vehicle injection, we suspected a prolonged effect of the injection. Indeed, this was supported by evaluating fluorescence signals from the mPFC recorded in rCPT before, during and after the Latin Square, with and without injections (Supplementary Fig. 5A). In sessions with vehicle injections (Supplementary Fig. S5A and C), the NA release signature showed a shallower dip following the dual peak when compared to sessions in stage 3 without any prior injection (Supplementary Fig. S5B and D). We therefore used the NA release signature after vehicle injection (Fig. 5B) as reference.

The data obtained after CNO injection was analyzed in two separate intervals: from rCPT start to minute 5 (early interval before the full effect of CNO), and from minute 5 to the end of the rCPT session (late interval when CNO expectably exerted its maximal effect) (Fig. 5A). During the early interval, the NA signature was, as would be expected, discernable, although some blurring was apparent (Fig. 5C, left). In contrast, the NA release signature during the late interval became dose-dependently blurred with the characteristic dual-peak structure largely absent at the higher doses (Fig. 5C, right). In the LH, we observed a comparable time-dependent blunting of the hit-associated NA signature (Supplementary Fig. S6).

DISCUSSION

NA is known as an important neuromodulator of arousal and cognitive performance [10, 12, 55]. A classical theory is the inverted U-shaped relationship that has been proposed to exist between the overall NA tone and attentional performance, with either insufficient or excessive NA levels resulting in reduced to fully impaired performance [17, 21, 22]. Based on electrophysiological recording of LC neurons, Aston-Jones et al. [1] specifically

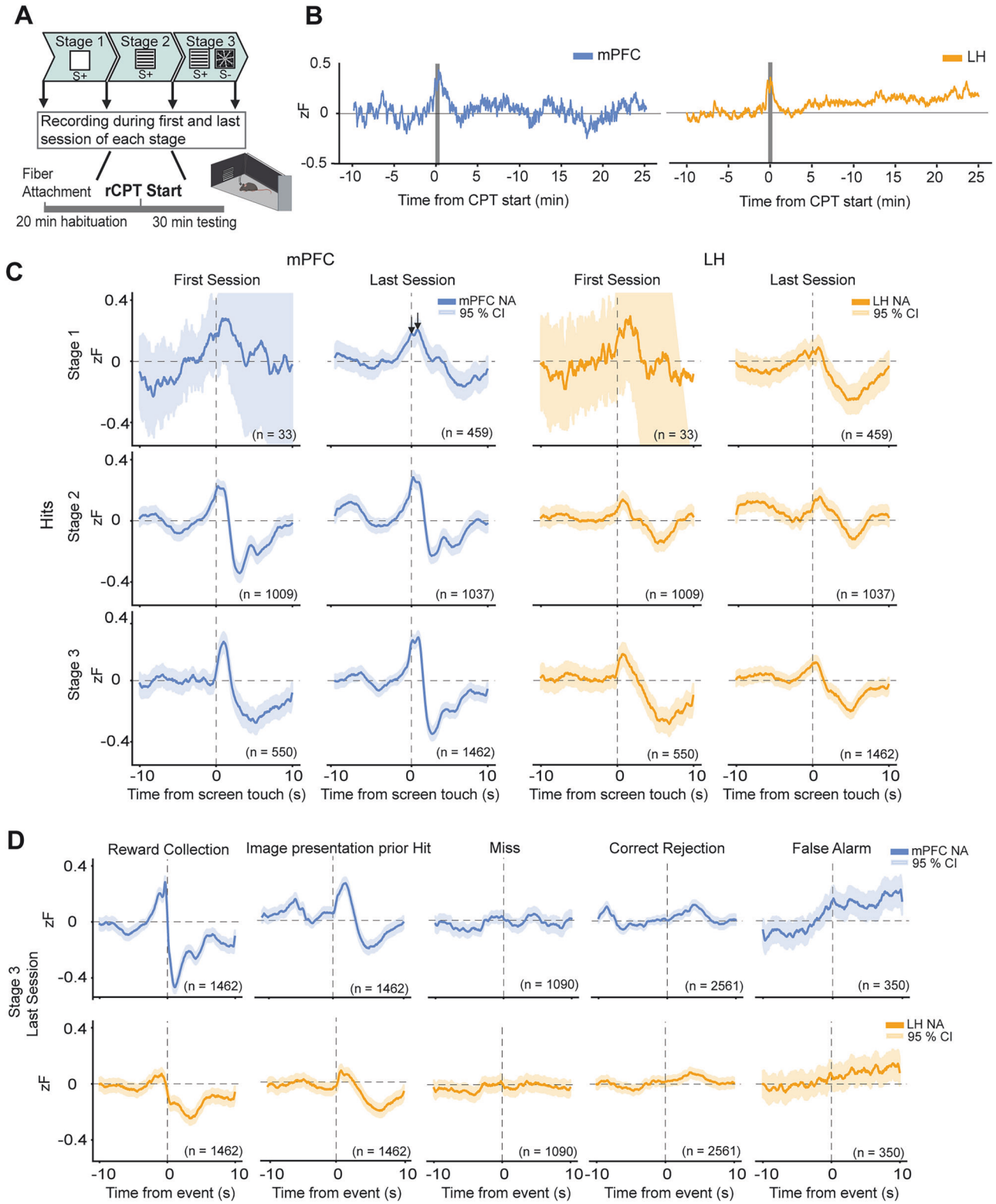

Fig. 3 Assessment of NA dynamics in mPFC and LH during CPT training (Stages 1-3) reveals release signatures time-locked to hits and reward. A Top: Overview of Stages 1–3 with timepoints of first and last recorded sessions. Bottom: Detailed testing timelines for each session. **B** Representative GRABNE2h (NA) traces (zF) from mPFC (blue) and LH (orange) during a Stage 3 training session, aligned to rCPT onset (time 0) with 10-min baseline. **C** Averaged NA signals (zF) across mice ($n = 20$), aligned to hits in the first and last sessions of Stages 1–3 (Stage 1 first session: $n = 8$). Left: mPFC (blue, shaded 95% CI); Right: LH (orange, shaded 95% CI). Dual peak in mPFC is marked in Stage 1 last session. Trial counts (number of hits) shown per plot. **D** Averaged NA signals in the final Stage 3 session, aligned to reward collection, miss, correct rejection, and false alarm. Top: mPFC (blue); Bottom: LH (orange), showing a weaker response. Shaded areas: 95% CI. Trial numbers indicated in each plot. For **C** and **D**, event-aligned traces are within-animal trial averages computed across many trials per condition (trial counts indicated in each plot).

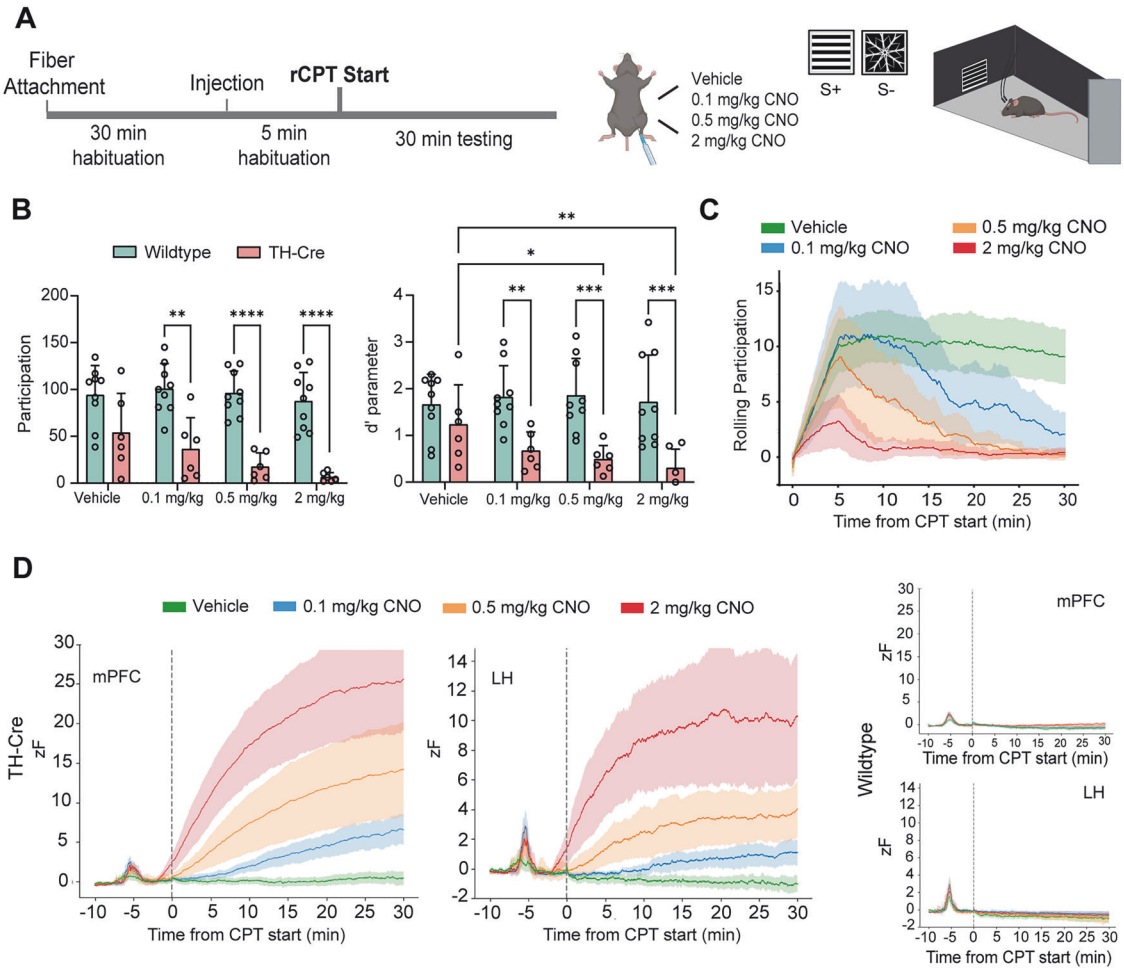

Fig. 4 Chemogenetic activation of LC promotes NA release in mPFC and LH and results in a dose-dependent decrease in rCPT performance in Stage 3. A Left: Timeline for Stage 3 testing and photometry. Mice received vehicle or CNO (0.1, 0.5, or 2 mg/kg) i.p., were placed in the CPT chamber after 5 min, and began the task following a 5-min habituation. Right: Illustration of Stage 3 target (S +) and non-target (S–) stimuli. **B** Behavioral performance of TH-Cre (coral, $n = 6$) and wildtype (teal, $n = 9$) mice. Left: Participation (Trials responded (hits + false alarms); Right: Discriminability (d′) . Data are mean ± SD. Two-way ANOVA with Tukey's test ($p < 0.05$, $p < 0.01$, $p < 0.001$, $p < 0.0001$) showed effects of dose (d′: F (3, 39) = 2.85, $p = 0.0496$; participation: F (1.83, 23.85) = 5.47, $p = 0.0128$), genotype (d′: F (1, 13) = 11.51, $p = 0.0048$; participation: F (1, 13) = 30.99, $p < 0.0001$), and dose × genotype interactions (d′: $p = 0.008$; participation: $p = 0.0304$). Genotype differences were significant at all doses; within TH-Cre mice, d′ differed between vehicle and 0.5 mg/kg ($p = 0.0150$) and 2 mg/kg ($p = 0.0017$). **C** Cumulative participation across the 30-min CPT in TH-Cre mice (5-min bins; whenever a hit is performed, 1 is added; when a mistake is performed, 1 is subtracted), thereby integrating performance over many trials across the session. Responding reduced with increasing CNO dose. Shaded areas: SD. **D** NA fiber photometry (zF) in mPFC and LH, aligned to task onset (0 min; injection at −5 min). CNO induced a dose-dependent increase in TH-Cre mice not seen in wildtypes. Colors: vehicle (green), 0.1 mg/kg (blue), 0.5 mg/kg (orange), 2 mg/kg (red). Shaded areas: 95% CI.

linked optimal attentional performance to intermediate tonic LC activity and phasic, target-specific LC responses [1]. Consistently, by directly assessing NA release, we show here data substantiating that attentional performance both depends on a balanced tonic NA tone [17, 22] and on the temporal precision and task-aligned dynamics of NA on a sub-second time scale. Indeed, the rise in tonic NA and concomitant blurring of phasic signatures upon chemogenetic activation of LC agree with the Aston-Jones inverted U-shape model that describes a shift from phasic to tonic mode at high NA levels accompanied by impairment of attentional performance [1]. Interestingly, reduced phasic LC responsiveness was seen also under CRF-increased tonic firing, suggesting that tonic-phasic tradeoffs may reflect an intrinsic physiological property of the LC rather than being specific to attention tasks [56].

Until recently, it was not feasible to capture real-time NA release dynamics on a fast time scale. The development of new genetically encoded NA sensors therefore represented a breakthrough in our ability to measure NA release [39, 40]. By combining viral expression of these sensors in desired target regions with fiber photometry, fast release dynamics can now be monitored over extended periods [39, 40, 49]. Importantly, the $GRAB_{NE2h}$ sensor was validated to reliably detect rapid NA changes in vivo including within the LH [40]. We therefore employed this sensor to investigate NA release dynamics during the rodent continuous performance task (rCPT), a learned task which is designed to assess attentional performance in mice while being translational to CPT performance in humans [43, 44]. We expressed the sensor in LH and mPFC, and during our subsequent fiber photometry experiments in the rCPT, we observed the development of NA release signatures in both regions associated with rewarded responses. The signatures exhibited a more defined temporal structure and were more prominent in the mPFC compared to the LH. This might reflect region-specific functions with the mPFC playing a central role in sustaining attention and top-down cognitive control [12, 55] and the LH being more

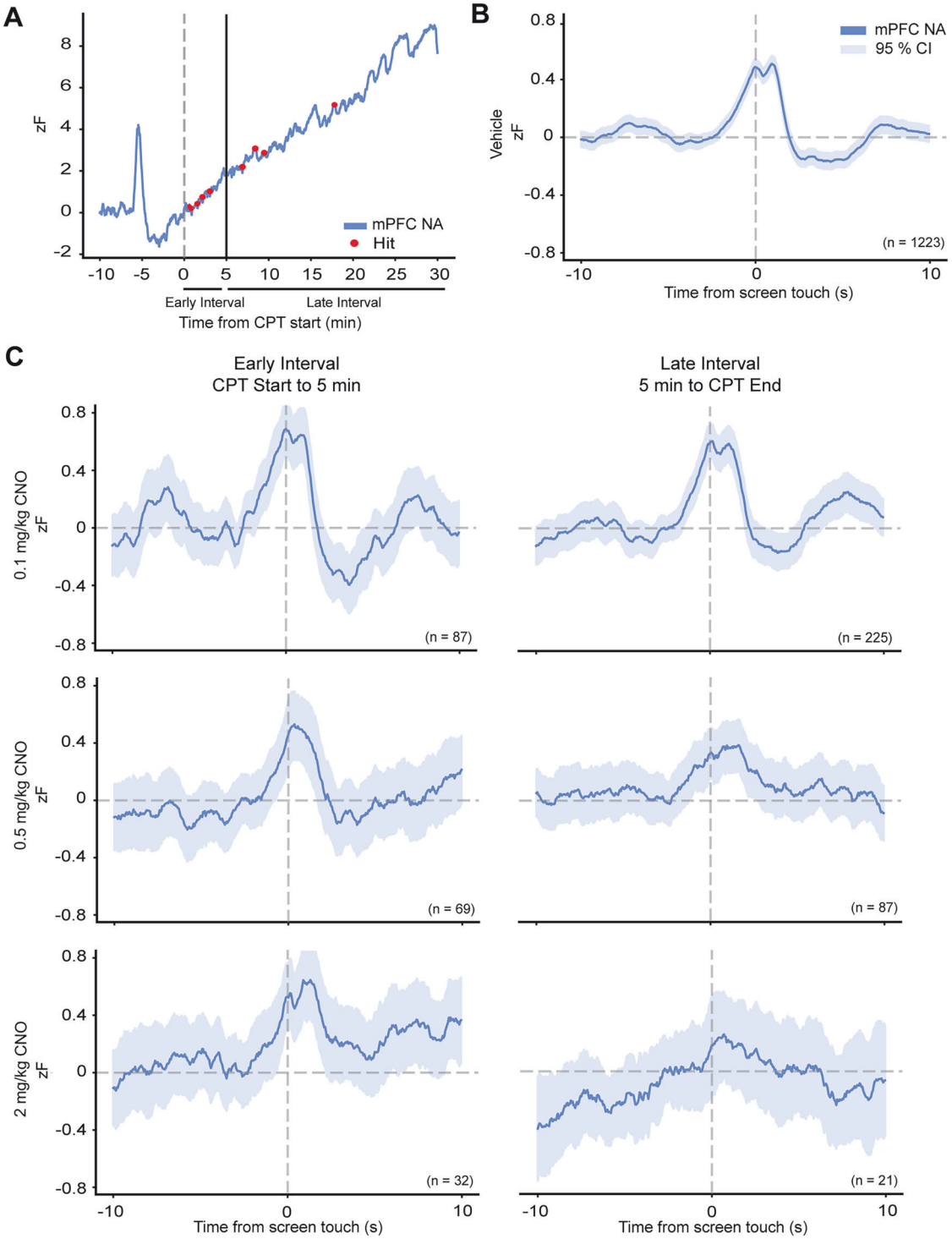

Fig. 5 Chemogenetic activation of the LC causes dose- and time-dependent blunting of the hit-associated NA release signature in the mPFC. A Representative mPFC NA signal (zF) aligned to rCPT start (time 0) in a TH-Cre mouse expressing hM3DGq, following CNO (2 mg/kg) injection. Red dots mark hit events. The vertical dashed line indicates the 5-min division used to segment each session into an early (rCPT Start to minute 5) and a late (minute 5 to rCPT End) interval. **B** Hit-aligned mPFC NA signal (zF) in TH-Cre mice ($n = 6$) under vehicle condition, serving as a reference NA release signature. **C** Hit-aligned mPFC NA signals in TH-Cre mice ($n = 6$), separated by interval. Early Interval (left column): The peak structure is still preserved, especially at lower doses. Late interval (right column): Responses are increasingly blunted, with the characteristic dual-peak largely absent, particularly at 0.5 and 2 mg/kg CNO. Shaded areas: 95% CI. Number of hits per condition shown in each plot.

broadly involved in arousal, stress, and motivational states [51, 57]. In this context, it is interesting that NA innervation of LH arises largely outside the LC [58–60], indicating that LC neurons are particularly responsive to task-related stimuli.

The signature associated with rewarded correct responses (hits) in the mPFC was characterized by a sharp increase upon target image presentation followed by an apparent dual peak. While the first of these occurred at the touch of the screen upon image

presentation, the second occurred when the mouse entered the reward tray for reward collection. Notably, the signature signal became more refined with training stage progression, yet less pronounced when uncertainty was introduced (e.g. going from Stage 2 to 3), altogether suggesting a learning-dependent shaping of the NA response. Importantly, there was no detectable signature associated with misses, correct rejections and false alarms (mistakes). The distinct shape of the hit-associated signature, and its refinement upon learning, suggest a critical role of temporally controlled NA release in attentional performance. Specifically, it is plausible to suggest that the signature - peaking before and dropping at reward collection - encodes a reward expectation that serves to promote task action and thereby optimizes test performance. The signature might also facilitate feedback integration, enhancing alertness to learned, reward-predictive stimuli and supporting more accurate stimulus discrimination. These interpretations align with a recent study using a graded auditory stimulus task, which proposed that LC-NA activity dynamics during learned behavior can facilitate task execution as well as encode reinforcement to improve performance [11]. It also aligns with data showing that optogenetic LC stimulations before the appearance of the target stimulus in a "two choice" task increased correct responses and decreased premature responses [38]. An alternative but not mutually exclusive interpretation is that the release signature reflects the salience of reward-prediction cues and action-outcome events [11, 40, 61, 62]. It might also be considered that the sharp decline around reward collection reflects transient suppression of LC-NA activity during consummatory behavior [61]. However, our animals were food-restricted, and the operant reward context differs from natural feeding behavior. Another lingering question is which inputs shape LC output during the rCPT. Interestingly, prefrontal regions send descending projections to the LC and can exert excitatory influence on LC neurons, providing a plausible route by which task demands, and outcome feedback could bias LC state and NA release timing [5, 63–65]. In line with this idea, recent work in the rCPT suggests that selective engagement of a mPFC to LC circuit can modulate attentional performance [66].

Chemogenetic hM3DGq-based LC activation with CNO caused a clear, dose-dependent increase in tonic NA levels in both mPFC and LH of the TH-Cre mice but not in WT control mice. Of note, a previous study observed similar profound increases in overall NA levels upon chemogenetic stimulation of LC neurons [67]. These rather dramatic effects seen even at low concentration of CNO are rarely quantified in DREADD activation experiments but important to bear in mind when concluding from chemogenetic studies with overexpression of Gq-based DREADDs particularly when interpreting e.g. inverted-U and adaptive gain models of LC-NA function. In addition, particularly at high CNO doses, the sustained LC activation could cause co-release of neuropeptides such as galanin [68]. It also is possible that the NA levels even exceed natural arousal responses; however, if the NA release peak in response to the injection ($t = 0$, Figs. 2B, C and 4D) can be considered a natural stress response (yet unlikely a maximum response), the NA levels seen for 0.1 mg/kg CNO are clearly physiological. We should moreover note that expression of hM3DGq appeared not to be fully confined to TH + LC neurons and extending into peri-LC areas (Supplementary Fig. S1); therefore, the behavioral effects of CNO might not be exclusively attributed to activation of LC-NA neurons. However, the $GRAB_{NE}$ recordings directly demonstrated a robust, dose-dependent elevation of tonic NA after CNO administration in TH-Cre mice, whereas WT (Cre-negative) control mice showed no detectable reporter expression and no comparable CNO-induced NA changes or behavioral phenotype. This argues against nonspecific CNO effects and shows that increased NA tone is a verified consequence of the manipulation and likely a major contributing factor to the observed phenotype.

Our detected increases in NA release were accompanied by a marked decrease in attentional performance even at the lowest CNO dose (0.1 mg/kg) with decreased d' parameter and overall decreased task participation. As stated above, this appears consistent with the theory of an inverted U-shaped relationship where too high tonic levels impair performance [17, 19, 22]. Our data widen this framework by showing that the impairment in task performance, and hence visual attention, also was paralleled by blurring of the characteristic and hit-associated NA signature pattern in the mPFC, supporting the conceivable importance of fast-scale NA release dynamics for attentional performance. We should note, however, a reduction in task participation upon chemogenetic LC activation was seen before in a patch-foraging task [69]. Changes in d' should therefore be interpreted cautiously, as reduced engagement can lower hit rates and thereby reduce d' even if discrimination accuracy is not selectively impaired. Hence, our findings at higher CNO doses might relate to reduced goal-directed attentional engagement rather than a selective attention deficit. Finally, the increase in NA in both the mPFC and LH reflects global chemogenetic LC activation and a subsequent widespread NA release across the entire brain. Thus, we cannot exclude possible roles of NA release dynamics in other brain regions than LH and mPFC.

Although chemogenetic LC-NA activation caused substantial increases in NA levels, we observed no changes in basic locomotor parameters, supporting that the impaired performance in response to LC-NA activation is not the result of disrupted motor functions or even sedation. We have no immediate explanation for previous findings indicating decreased motor activity upon chemogenetic LC-NA activation [70, 71]. We did observe, however, that the mice spent less time in the center zone of the open field arena, which is indicative of anxiety-like behavior [53, 54] and consistent with previous observations showing that elevated NA levels can elicit this phenotype [57, 70, 72]. Nonetheless, in our experiments, the open-field arena was a novel and potentially anxiogenic context compared to the rCPT chambers with which the mice were highly familiar after repeated exposure throughout the study.

In summary, our findings suggest that LC-mediated NA release in the mPFC and LH, as well as possibly in other brain regions, conveys behaviorally relevant information through dynamic, time-locked signaling patterns that are synchronized with attentional and goal-directed behaviors. The results substantiate thereby a key role of sub-second NA release dynamics in attentional behavior and set the stage for future investigations of how these dynamics might be altered in cognitive disorders, such as ADHD and depression [12, 73, 74]. Furthermore, they open avenues for exploring how such alterations might be pharmacologically mitigated.

DATA AVAILABILITY

The raw data that support the findings of this study are available from the corresponding author upon request.

REFERENCES

1. Aston-Jones G, Rajkowski J, Cohen J. Locus coeruleus and regulation of behavioral flexibility and attention. Prog Brain Res. 2000;126:165–82. https://doi.org/10.1016/S0079-6123(00)26013-5.
2. Schwarz LA, Miyamichi K, Gao XJ, Beier KT, Weissbourd B, DeLoach KE, et al. Viral-genetic tracing of the input-output organization of a central noradrenaline circuit. Nature. 2015;524:88–92. https://doi.org/10.1038/nature14600.
3. Poe GR, Foote S, Eschenko O, Johansen JP, Bouret S, Aston-Jones G, et al. Locus coeruleus: a new look at the blue spot. Nat Rev Neurosci. 2020;21:644–59. https://doi.org/10.1038/s41583-020-0360-9.
4. Chandler DJ, Gao WJ, Waterhouse BD. Heterogeneous organization of the locus coeruleus projections to prefrontal and motor cortices - PubMed. Proc Natl Acad Sci USA. 2014;111:6816–21. https://doi.org/10.1073/pnas.1320827111.

5. Aston-Jones G, Cohen JD. An integrative theory of locus coeruleus-norepinephrine function: adaptive gain and optimal performance. Annu Rev Neurosci. 2005;28:403–50. https://doi.org/10.1146/annurev.neuro.28.061604.135709.
6. Thiele A, Bellgrove MA. Neuromodulation of Attention. Neuron. 2018;97:769–85. https://doi.org/10.1016/j.neuron.2018.01.008.
7. Berridge CW, Page ME, Valentino RJ, Foote SL. Effects of locus coeruleus inactivation on electroencephalographic activity in neocortex and hippocampus. Neuroscience. 1993;55:381–93. https://doi.org/10.1016/0306-4522(93)90507-C.
8. Sara SJ. The locus coeruleus and noradrenergic modulation of cognition. Nat Rev Neurosci. 2009;10:211–23. https://doi.org/10.1038/nrn2573.
9. Sara SJ, Bouret S. Orienting and reorienting: the locus coeruleus mediates cognition through arousal - PubMed. Neuron. 2012;76:130–41. https://doi.org/10.1016/j.neuron.2012.09.011.
10. Berridge CW. Noradrenergic modulation of arousal - PubMed. Brain Res Rev. 2008;58:1–17. https://doi.org/10.1016/j.brainresrev.2007.10.013.
11. Breton-Provencher V, Drummond GT, Feng J, Li Y, Sur M. Spatiotemporal dynamics of noradrenaline during learned behaviour. Nature. 2022;606:732–8. https://doi.org/10.1038/s41586-022-04782-2.
12. Robbins TW, Arnsten AFT. The neuropsychopharmacology of fronto-executive function: monoaminergic modulation. Annu Rev Neurosci. 2009;32:267–87. https://doi.org/10.1146/annurev.neuro.051508.135535.
13. Arnsten AFT, Rubia K. Neurobiological circuits regulating attention, cognitive control, motivation, and emotion: disruptions in neurodevelopmental psychiatric disorders - PubMed. J Am Acad Child Adolesc Psychiatry. 2012;51:356–67. https://doi.org/10.1016/j.jaac.2012.01.008.
14. Tait DS, Brown VJ, Farovik A, Theobald DE, Dalley JW, Robbins TW. Lesions of the dorsal noradrenergic bundle impair attentional set-shifting in the rat. Eur J Neurosci. 2007;25:3719–24. https://doi.org/10.1111/j.1460-9568.2007.05612.x.
15. Mcburney-Lin J, Vargova G, Garad M, Zagha E, Yang H. The locus coeruleus mediates behavioral flexibility. Cell Rep. 2022;41:111534. https://doi.org/10.1016/j.celrep.2022.111534.
16. Berridge CW, Arnsten AFT. Psychostimulants and motivated behavior: arousal and cognition - PubMed. Neurosci Biobehav Rev. 2013;37:1976–84. https://doi.org/10.1016/j.neubiorev.2012.11.005.
17. Arnsten AFT, Pliszka SR. Catecholamine influences on prefrontal cortical function: Relevance to treatment of attention deficit/hyperactivity disorder and related disorders. Pharmacol Biochem Behav. 2011;99:211–6. https://doi.org/10.1016/j.pbb.2011.01.020.
18. Gill TM, Sarter M, Givens B. Sustained Visual Attention Performance-Associated Prefrontal Neuronal Activity: Evidence for Cholinergic Modulation. J Neurosci. 2000;20:4745–57. https://doi.org/10.1523/jneurosci.20-12-04745.2000.
19. Jørgensen SH, Fitzpatrick CM, Gether U, Woldbye DPD, Sørensen AT. Chemogenetic Modulation of G Protein-Coupled Receptor Signalling in Visual Attention Research. Basic Clin Pharmacol Toxicol. 2017;121:373–81. https://doi.org/10.1111/bcpt.12819.
20. Carli M, Robbins TW, Evenden JL, Everitt BJ. Effects of lesions to ascending noradrenergic neurones on performance of a 5-choice serial reaction task in rats; implications for theories of dorsal noradrenergic bundle function based on selective attention and arousal. Behav Brain Res. 1983;9:361–80.
21. Arnsten AFT. Catecholamine modulation of prefrontal cortical cognitive function. Trends Cogn Sci. 1998;2:436–47. https://doi.org/10.1016/S1364-6613(98)01240-6.
22. Urban KR, Gao WJ. Performance enhancement at the cost of potential brain plasticity: neural ramifications of nootropic drugs in the healthy developing brain - PubMed. Front Syst Neurosci 2014;8. https://doi.org/10.3389/fnsys.2014.00038.
23. Del Campo N, Chamberlain SR, Sahakian BJ, Robbins TW. The roles of dopamine and noradrenaline in the pathophysiology and treatment of attention-deficit/hyperactivity disorder. Biol Psychiatry. 2011;69:e145–57. https://doi.org/10.1016/j.biopsych.2011.02.036.
24. Caballero-Puntiverio M, Lerdrup LS, Grupe M, Larsen CW, Dietz AG, Andreasen JT. Effect of ADHD medication in male C57BL/6J mice performing the rodent Continuous Performance Test - PubMed. Psychopharmacology. 2019;236:1839–51. https://doi.org/10.1007/s00213-019-5167-x.
25. Faraone SV, Spencer T, Aleardi M, Pagano C, Biederman J. Meta-Analysis of the Efficacy of Methylphenidate for Treating Adult Attention-Deficit/Hyperactivity Disorder. J Clin Psychopharmacol. 2004;24:24–29. https://doi.org/10.1097/01.jcp.0000108984.11879.95.
26. Turner KM, Burne THJ. Improvement of attention with amphetamine in low- and high-performing rats. Psychopharmacology. 2016;233:3383–94. https://doi.org/10.1007/s00213-016-4376-9.
27. Arnsten AFT. Stimulants: Therapeutic Actions in ADHD. Neuropsychopharmacology. 2006;31:2376–83. https://doi.org/10.1038/sj.npp.1301164.
28. Chandler D, and Waterhouse BD. Evidence for Broad Versus Segregated Projections from Cholinergic and Noradrenergic Nuclei to Functionally and Anatomically Discrete Subregions of Prefrontal Cortex. Fronti Behav Neurosci 2012;6. https://doi.org/10.3389/fnbeh.2012.00020.
29. Chandler DJ, Lamperski CS, Waterhouse BD. Identification and distribution of projections from monoaminergic and cholinergic nuclei to functionally differentiated subregions of prefrontal cortex. Brain Res. 2013;1522:38–58. https://doi.org/10.1016/j.brainres.2013.04.057.
30. Milstein JA, Lehmann O, Theobald DEH, Dalley JW, Robbins TW. Selective depletion of cortical noradrenaline by anti-dopamine beta-hydroxylase–saporin impairs attentional function and enhances the effects of guanfacine in the rat. Psychopharmacology. 2006;190:51–63. https://doi.org/10.1007/s00213-006-0594-x.
31. Dalley JW, Cardinal RN, Robbins TW. Prefrontal executive and cognitive functions in rodents: neural and neurochemical substrates. Neurosci Biobehav Rev. 2004;28:771–84. https://doi.org/10.1016/j.neubiorev.2004.09.006.
32. Jones DT, Graff-Radford J. Executive Dysfunction and the Prefrontal Cortex - PubMed. Contin. 2021;27:1586–601. https://doi.org/10.1212/CON.0000000000001009.
33. Solbakk AK, Løvstad M. Effects of focal prefrontal cortex lesions on electrophysiological indices of executive attention and action control - PubMed. Scand J Psychol. 2014;55:233–43. https://doi.org/10.1111/sjop.12106.
34. McGaughy J, Ross RS, Eichenbaum H. Noradrenergic, but not cholinergic, deafferentation of prefrontal cortex impairs attentional set-shifting. Neuroscience. 2008;153:63–71. https://doi.org/10.1016/j.neuroscience.2008.01.064.
35. Dalley JW, McGaughy J, O'Connell MT, Cardinal RN, Levita L, Robbins TW. Distinct changes in cortical acetylcholine and noradrenaline efflux during contingent and noncontingent performance of a visual attentional task. J Neurosci Off J Soc Neurosci. 2001;21:4908–14.
36. Newman LA, Darling J, McGaughy J. Atomoxetine reverses attentional deficits produced by noradrenergic deafferentation of medial prefrontal cortex. Psychopharmacology. 2008;200:39–50. https://doi.org/10.1007/s00213-008-1097-8.
37. Hallock HL, Adiraju SS, Miranda-Barrientos J, Mcinerney JM, Oh S, Debrosse AC, et al. Electrophysiological correlates of attention in the locus coeruleus–prelimbic cortex circuit during the rodent continuous performance test. Neuropsychopharmacology. 2024;49:521–31. https://doi.org/10.1038/s41386-023-01692-3.
38. Bari A, Xu S, Pignatelli M, Takeuchi D, Feng J, Li Y, et al. Differential attentional control mechanisms by two distinct noradrenergic coeruleo-frontal cortical pathways. Proc Natl Acad Sci USA. 2020;117:29080–9. https://doi.org/10.1073/pnas.2015635117.
39. Feng J, Zhang C, Lischinsky JE, Jing M, Zhou J, Wang H, et al. A Genetically Encoded Fluorescent Sensor for Rapid and Specific In Vivo Detection of Norepinephrine. Neuron. 2019;102:745–.e8. https://doi.org/10.1016/j.neuron.2019.02.037.
40. Feng J, Dong H, Lischinsky JE, Zhou J, Deng F, Zhuang C, et al. Monitoring norepinephrine release in vivo using next-generation GRABNE sensors. Neuron. 2024;112:1930–.e6. https://doi.org/10.1016/j.neuron.2024.03.001.
41. Roth BL. DREADDs for Neuroscientists - PubMed. Neuron. 2016;89:683–94. https://doi.org/10.1016/j.neuron.2016.01.040.
42. Urban DJ, Roth BL. DREADDs (designer receptors exclusively activated by designer drugs): chemogenetic tools with therapeutic utility - PubMed. Annu Rev Pharmacol Toxicol. 2015;55:399–417. https://doi.org/10.1146/annurev-pharmtox-010814-124803.
43. Kim CH, Hvoslef-Eide M, Nilsson SRO, Johnson MR, Herbert BR, Robbins TW, et al. The continuous performance test (rCPT) for mice: a novel operant touchscreen test of attentional function - PubMed. Psychopharmacology. 2015;232:3947–66. https://doi.org/10.1007/s00213-015-4081-0.
44. Roberts BZ, Young JW. Translational cognitive systems: focus on attention. Emerg Top Life Sci. 2022;6:529–39. https://doi.org/10.1042/etls20220009.
45. Fisher BM, Saksida LM, Robbins TW, Bussey TJ. Functional dissociations between subregions of the medial prefrontal cortex on the rodent touchscreen continuous performance test (rCPT) of attention - PubMed. Behav Neurosci. 2020;134:1–14. https://doi.org/10.1037/bne0000338.
46. Savitt JM, Jang SS, Mu W, Dawson VL, Dawson TM. Bcl-x is required for proper development of the mouse substantia nigra. J Neurosci. 2005;25:6721–8. https://doi.org/10.1523/jneurosci.0760-05.2005.
47. Runegaard AH, Jensen KL, Fitzpatrick CM, Dencker D, Weikop P, Gether U, et al. Preserved dopaminergic homeostasis and dopamine-related behaviour in hemizygous TH-Cre mice. Eur J Neurosci. 2017;45:121–8. https://doi.org/10.1111/ejn.13347.
48. Lopes, G, Bonacchi, N, FrazÃ£o, J, Neto, JP, Atallah, BV, Soares, S, et al. Bonsai: an event-based framework for processing and controlling data streams. Front Neuroinf 2015;9. https://doi.org/10.3389/fninf.2015.00007.
49. Simpson EH, Akam T, Patriarchi T, Blanco-Pozo M, Burgeno LM, Mohebi A, et al. Lights, fiber, action! A primer on in vivo fiber photometry. Neuron. 2024;112:718–39. https://doi.org/10.1016/j.neuron.2023.11.016.
50. McQuade R, Stanford SC. A microdialysis study of the noradrenergic response in rat frontal cortex and hypothalamus to a conditioned cue for aversive, naturalistic environmental stimuli. Psychopharmacology. 2000;148:201–8. https://doi.org/10.1007/s002130050043.

51. Biro L, Sipos E, Bruzsik B, Farkas I, Zelena D, Balazsfi D, et al. Task Division within the Prefrontal Cortex: Distinct Neuron Populations Selectively Control Different Aspects of Aggressive Behavior via the Hypothalamus - PubMed. J Neurosci Off J Soc Neurosci. 2018;38:4065–75. https://doi.org/10.1523/JNEUROSCI.3234-17.2018.
52. Armbruster BN, Li X, Pausch MH, Herlitze S, Roth BL. Evolving the lock to fit the key to create a family of G protein-coupled receptors potently activated by an inert ligand - PubMed. Proc Natl Acad Sci USA. 2007;104:5163–8. https://doi.org/10.1073/pnas.0700293104.
53. Prut L, Belzung C. The open field as a paradigm to measure the effects of drugs on anxiety-like behaviors: a review. Eur J Pharmacol. 2003;463:3–33. https://doi.org/10.1016/S0014-2999(03)01272-X.
54. Kraeuter AK, Guest PC, Sarnyai Z. The Open Field Test for Measuring Locomotor Activity and Anxiety-Like Behavior - PubMed. Methods Mol Biol. 2019;1916:99–103. https://doi.org/10.1007/978-1-4939-8994-2_9.
55. Holland N, Robbins TW, Rowe JB. The role of noradrenaline in cognition and cognitive disorders. Brain. 2021;144:2243–56. https://doi.org/10.1093/brain/awab111.
56. Valentino R, Foote S. Corticotropin-releasing hormone increases tonic but not sensory-evoked activity of noradrenergic locus coeruleus neurons in unanesthetized rats. J Neurosci. 1988;8:1016–25. https://doi.org/10.1523/JNEUROSCI.08-03-01016.1988.
57. Tanaka M, Yoshida M, Emoto H, Ishii H. Noradrenaline systems in the hypothalamus, amygdala and locus coeruleus are involved in the provocation of anxiety: basic studies. Eur J Pharmacol. 2000;405:397–406. https://doi.org/10.1016/S0014-2999(00)00569-0.
58. Palkovits M, Záborszky L, Feminger A, Mezey É, Fekete MIK, Herman JP, et al. Noradrenergic innervation of the rat hypothalamus:experimental biochemical and electron microscopic studies. Brain Res. 1980;191:161–71. https://doi.org/10.1016/0006-8993(80)90320-0.
59. Fritschy JM, Grzanna R. Immunohistochemical analysis of the neurotoxic effects of DSP-4 identifies two populations of noradrenergic axon terminals. Neuroscience. 30:181–97. https://doi.org/10.1016/0306-4522(89)90364-3.
60. Robertson SD, Plummer NW, De Marchena J, Jensen P. Developmental origins of central norepinephrine neuron diversity. Nat Neurosci. 2013;16:1016–23. https://doi.org/10.1038/nn.3458.
61. Sciolino NR, Hsiang M, Mazzone CM, Wilson LR, Plummer NW, Amin J, et al. Natural locus coeruleus dynamics during feeding. Sci Adv. 2022;8:eabn9134. https://doi.org/10.1126/sciadv.abn9134.
62. Foote SL, Aston-Jones G, Bloom FE. Impulse activity of locus coeruleus neurons in awake rats and monkeys is a function of sensory stimulation and arousal. Proc Natl Acad Sci USA. 1980;77:3033–7. https://doi.org/10.1073/pnas.77.5.3033.
63. Jodoj E, Chiang C, Aston-Jones G. Potent excitatory influence of prefrontal cortex activity on noradrenergic locus coeruleus neurons. Neuroscience. 1998;83:63–79. https://doi.org/10.1016/s0306-4522(97)00372-2.
64. Arnsten AFT, Goldman-Rakic PS. Selective prefrontal cortical projections to the region of the locus coeruleus and raphe nuclei in the rhesus monkey. Brain Res. 1984;ume 306:9–18. https://doi.org/10.1016/0006-8993(84)90351-2.
65. Lu Y, Simpson KL, Weaver KJ, Lin RCS. Differential distribution patterns from medial prefrontal cortex and dorsal raphe to the locus coeruleus in rats. Neuroscience. 2012;ume295:1192–201. https://doi.org/10.1002/ar.22505.
66. Rehg JJ, Olivares DE, Li Y, Martinowich K, Carr GV, and Miranda-Barrientos J. Top-down control of sustained attention by the medial prefrontal cortex (mPFC) - locus coeruleus (LC) circuit during the rodent continuous performance test (rCPT). bioRxiv [Preprint]. 2025. https://doi.org/10.64898/2025.12.01.691673.
67. Oyarzabal EA, Hsu L-M, Das M, Chao T-HH, Zhou J, Song S, et al. Chemogenetic stimulation of tonic locus coeruleus activity strengthens the default mode network. Sci Adv 2022;8. https://doi.org/10.1126/sciadv.abm9898.
68. Tillage RP, Foster SL, Lustberg D, Liles LC, McCann KE, Weinshenker D. Co-released norepinephrine and galanin act on different timescales to promote stress-induced anxiety-like behavior. Neuropsychopharmacology. 2021;46:1535–43. https://doi.org/10.1038/s41386-021-01011-8.
69. Kane GA, Vazey EM, Wilson RC, Shenhav A, Daw ND, Aston-Jones G, et al. Increased locus coeruleus tonic activity causes disengagement from a patch-foraging task. Cogn Affect Behav Neurosci. 2017;17:1073–83. https://doi.org/10.3758/s13415-017-0531-y.
70. McCall JG, Siuda ER, Bhatti DL, Lawson LA, McElligott ZA, Stuber GD, et al. Locus coeruleus to basolateral amygdala noradrenergic projections promote anxiety-like behavior. eLife 2017;6. https://doi.org/10.7554/eLife.18247.
71. Zerbi V, Floriou-Servou A, Markicevic M, Vermeiren Y, Sturman O, Privitera M, et al. Rapid Reconfiguration of the Functional Connectome after Chemogenetic Locus Coeruleus Activation. Neuron. 2019;103:702–.e5. https://doi.org/10.1016/j.neuron.2019.05.034.
72. Ressler KJ, Nemeroff CB. Role of serotonergic and noradrenergic systems in the pathophysiology of depression and anxiety disorders. Depress Anxiety. 2000;12:2–19.
73. Russell VA, Sagvolden T, Johansen EB. Animal models of attention-deficit hyperactivity disorder. Behav Brain Funct: BBF. 2005;1:9 https://doi.org/10.1186/1744-9081-1-9.
74. Arnsten AFT. The Emerging Neurobiology of Attention Deficit Hyperactivity Disorder: The Key Role of the Prefrontal Association Cortex. J Pediatr. 2009;154:I–S43. https://doi.org/10.1016/j.jpeds.2009.01.018.

ACKNOWLEDGEMENTS

We thank Dr. Yulong Li, Peking University for providing the $GRAB_{NE2h}$ sensor and thank Anette Dencker Kaas for excellent technical assistance.

AUTHOR CONTRIBUTIONS

L.P.P., S.H.J., F.H. A.T.S. and U.G. conceptualized the study. L.P.P., J.C.M., S.H.J., A.T.S. and U.G. designed experiments. L.P.P., J.C.M., K.K., J.M. and S.O. carried out experiments, L.P.P., S.H.J., J.C.M. and S.H.E. performed data analysis. L.P.P., J.C.M., S.H.J., F.H. T.W.R. J.W.D. and U.G. interpreted data. L.P.P. and U.G. wrote the manuscript in consultation with all authors.

FUNDING

The work was supported by the Lundbeck Foundation R6-2017-4331 (UG), R276-2018-792 (UG), R359-2020-2301 (UG), R181-2014-3090 (FH) and R303-2018-3540 (FH). Open access funding provided by Copenhagen University.

COMPETING INTERESTS

The authors declare no competing interests.

ADDITIONAL INFORMATION

Supplementary information The online version contains supplementary material available at https://doi.org/10.1038/s41386-026-02404-3.

Correspondence and requests for materials should be addressed to Ulrik Gether.

Reprints and permission information is available at http://www.nature.com/reprints

Publisher's note Springer Nature remains neutral with regard to jurisdictional claims in published maps and institutional affiliations.